FULL PAPER

Dalton
www.rsc.org/dalton

Nanoclusters of phenylphosphonium cations and cyanoferrate anions in the gas phase, and the principles of association of these ions in crystals

Philip A. W. Dean,*[a] Keith Fisher,[b] Don Craig,[b] Michael Jennings,[a] Ohenewa Ohene-Fianko,[a] Marcia Scudder,[b] Gary Willett[b] and Ian Dance *[b]

[a] *Department of Chemistry, University of Western Ontario, London, Ontario N6A 5B7, Canada*
[b] *School of Chemical Sciences, University of New South Wales, Sydney NSW 2052, Australia*

Received 20th December 2002, Accepted 17th February 2003
First published as an Advance Article on the web 10th March 2003

Electrospray Fourier transform mass spectrometry of combinations of the cations $MePh_3P^+$ or Ph_4P^+ with the anions $[Fe(CN)_6]^{3-}$ or $[Fe(CN)_5(NO)]^{2-}$ in methanol yields a rich collection of aggregates, mainly with net negative charge. 23 anionic aggregates of $MePh_3P^+$ and $[Fe(CN)_6]^{3-}$ range in size from $[(MePh_3P^+)_2[Fe(CN)_6]^{3-}]^-$ to $[(MePh_3P^+)_{37}\{[Fe(CN)_6]^{3-}\}_{14}]^{5-}$, while 23 anionic aggregates of Ph_4P^+ and $[Fe(CN)_6]^{3-}$ range up to $[(Ph_4P^+)_{38}\{[Fe(CN)_6]^{3-}\}_{15}]^{7-}$. The compositions of the anionic aggregates tend towards cation/anion ratios that yield a charge density of −0.15 per component species. Structural principles which may be applicable to these gaseous nanoclusters have been investigated *via* analysis of the crystal packing in four new crystal structures of salts containing phenylphosphonium cations and cyanoferrate anions which have stoichiometries that span the same cation/anion ratios. They are $(Ph_4P)_3[Fe(CN)_6](H_2O)(BuOH)(hexane)$, $(Me_2Ph_2P)_3[Fe(CN)_6](H_2O)_2$, $(MePh_3P)_2[Fe(CN)_5(NO)](H_2O)_2$ and $(Ph_4P)_2[Fe(CN)_5(NO)]$. In the solids there is general dispersal of oppositely charged ions, consistent with the overall electrostatics, but also numerous and prevalent hydrogen bonds between phenyl C–H of the cations and coordinated CN^- (and NO) of the anionic metal complexes. Multiple phenyl embraces, often formed by these cations, are not influential in these crystals. Density functional calculation of the energies of the charge-assisted C–H ··· NC hydrogen bonds (*ca.* 4 kcal mol^{-1}), and estimates of ion ··· ion electrostatic energies, lead to the general conclusion that in the gas-phase ion-aggregates the net electrostatic energies and the net hydrogen bonding energies are dominant and of similar magnitude. Models of the clusters of molecular ions indicate that their diameters are 3–4 nm for $[(Ph_4P^+)_{19}\{[Fe(CN)_6]^{3-}\}_8]^{5-}$ and 4–5 nm for $[(Ph_4P^+)_{38}\{[Fe(CN)_6]^{3-}\}_{15}]^{7-}$.

Introduction

Anionic cyanometallate complexes are fundamental components of many newly fabricated materials with significant inclusion[1] and magnetic properties.[2] Amphiphilic pentacyanoferrate(III) complexes have been used to generate and stabilise Langmuir–Blodgett films,[3] and a recent publication describes a lamellar anionic cyano-cuprate network with intercalating Ph_4P^+ cations.[4]

We are investigating the patterns and principles for association of cyanometallate anions with themselves and with their counter-cations. The principles we seek encompass both the geometric and the energetic aspects of association. One relevant experimental technique is electrospray mass spectrometry (ESMS),[5] which is significant because it reveals cation ··· anion associations, desolvated from solution, and we have used ESMS previously to investigate the $Bu_4N^+Br^-$ system.[6] In this paper we report ESMS results for the cyanoferrate anions $[Fe(CN)_6]^{3-}$ and $[Fe(CN)_5(NO)]^{2-}$, accompanied by phenylphosphonium cations Ph_4P^+ and $MePh_3P^+$. More than 50 aggregates are observed, ranging in size up to $[(Ph_4P)_{38}\{Fe(CN)_6\}_{15}]^{7-}$ which is 4–5 nm in diameter. There is very little prior work on cyanoferrates in the gas phase.[7]

We selected phenylphosphonium cations because they are also remarkably successful for the crystallisation of anions, and it is now recognised that this is at least partly due to the presence of favourable intermolecular interactions between phenylated cations in the form of multiple phenyl embraces.[8] In order to generate structural information not provided by the ESMS results, we also report here the crystal structures of the four new compounds $(Ph_4P)_3[Fe(CN)_6](H_2O)(BuOH)(hexane)$, $(Me_2Ph_2P)_3[Fe(CN)_6](H_2O)_2$, $(MePh_3P)_2[Fe(CN)_5(NO)](H_2O)_2$ and $(Ph_4P)_2[Fe(CN)_5(NO)]$, and analyse the crystal packing in search of the geometric principles for association of cyanoferrate anions and phenylphosphonium cations. There was only one relevant crystal structure in the Cambridge structural database.

The crystal packing analysis provides detailed geometric information about association of these molecular ions, but not the energies which determine these structures. Accordingly, some calculations of the relevant energies are reported.

A number of specific questions underly this investigation. Cyanometallate anions such as $[Fe(CN)_6]^{3-}$ and $[Fe(CN)_5(NO)]^{2-}$ have spikey surfaces: how does this affect their association, and are they shape-awkward or shape-auspicious? Do multiple phenyl embraces occur between the phenylphosphonium cations when associated with cyanometallate anions? The two anions have different charges, which changes the ratio (in number and volume) of cation and anion in the associates: what are the effects of this in the geometry of association? Is there significant hydrogen bonding to coordinated cyanide? What are the relative magnitudes of the intermolecular energies provided by ion electrostatics, multiple phenyl embraces, and hydrogen bonding? Any C–H ··· NC hydrogen bonding would be charge-assisted at both the (positive) donor and (negative) acceptor sides.

Experimental

Preparations of compounds and solutions

$(Me_2Ph_2P)_3[Fe(CN)_6](H_2O)_2$. $Ag_3[Fe(CN)_6]$ {made from 3 $AgNO_3$ + $K_3[Fe(CN)_6]$ in aqueous solution} (0.2088 g, 0.3899 mmol) was added to a stirred solution of Me_2Ph_2PI (Aldrich, 0.4001 g, 1.169 mmol) in EtOH (10 mL). Stirring was continued for 1 day, with the reaction mixture protected from light. The AgI was removed by centrifugation, and cyclohexane was layered on to a 1-mL portion of the yellow solution, to give the crystal used for X-ray diffraction analysis.

DOI: 10.1039/b212488b

Table 1 Crystallographic data for $(Ph_4P)_3[Fe(CN)_6](H_2O)(BuOH)(hexane)$, $(Me_2Ph_2P)_3[Fe(CN)_6](H_2O)_2$, $(MePh_3P)_2[Fe(CN)_5(NO)](H_2O)_2$ and $(Ph_4P)_2[Fe(CN)_5(NO)]$

Formula	$(Ph_4P)_3[Fe(CN)_6]$-$(H_2O)(BuOH)(hexane)$	$(Me_2Ph_2P)_3[Fe(CN)_6]$-$(H_2O)_2$	$(MePh_3P)_2[Fe(CN)_5(NO)]$-$(H_2O)_2$	$(Ph_4P)_2[Fe(CN)_5(NO)]$
Asymmetric unit	$C_{44}H_{43}Fe_{0.5}N_3OP_{1.5}$	$C_{48}H_{52}FeN_6O_2P_3$	$C_{21.5}H_{20}Fe_{0.5}N_3O_{1.5}P$	$C_{53}H_{40}FeN_6OP_2$
M	704.20	893.72	403.3	894.7
Crystal system	Orthorhombic	Monoclinic	Monoclinic	Monoclinic
Space group	*Pccn*	*P*2/*c*	$P2_1/c$	$P2_1/c$
a/Å	15.8694(3)	24.8172(4)	9.805(6)	8.993(7)
b/Å	17.6413(3)	9.1563(2)	12.026(3)	21.378(8)
c/Å	26.4893(5)	21.3197(4)	17.23(1)	24.32(2)
β/°	90	107.703(1)	90.27(3)	104.57(3)
V/Å^3	7415.9(2)	4615.1(2)	2032(2)	4526(4)
D_c/g cm^{-3}	1.26	1.29	1.32	1.31
Z	8	4	4	4
μ_{Mo}/mm^{-1}	0.322	0.476	0.492	0.445
Temperature/K	150(2)	150(2)	294(2)	294(2)
$2\theta_{max}$/°	50	60	50	46
Crystal decay	None	None	None	None
Min. transmission factor	0.91	0.83	0.90	0.92
Max. transmission factor	0.94	0.90	0.97	0.95
Unique refl.	6540	13480	3569	5892
Observed refl.	4877	7763	2758	4598
R_{merge}	0.056	0.051	0.010	0.009
R	0.065	0.046	0.041	0.033
R_w	0.177	0.125	0.057	0.045

$(Ph_4P)_3[Fe(CN)_6](H_2O)$(*n*-BuOH)(hexane). This was prepared in a similar manner to the preceding $Me_2Ph_2P^+$ salt, using Ph_4PI (0.1024 g, 0.214 mmol) and $Ag_3[Fe(CN)_6]$. Crystals were obtained by adding *n*-BuOH to a portion of the ethanolic solution and diffusing hexane into the mixture.

$(MePh_3P)_2[Fe(CN)_5(NO)](H_2O)_2$. A solution of $MePh_3PI$ (2.97 g, 7.3 mmol) in MeOH (5 mL) was added with stirring to a solution of $Na_2[Fe(CN)_5(NO)]\cdot 2H_2O$ (1.00 g, 3.4 mmol) in water (5 mL). The precipitate that is initially formed dissolved as more of the methanolic solution was added. Addition of a further 5 mL of water produced a red–brown oil. Cooling the mixture in ice and scratching the oil with a glass rod, produced a solid product. This pink–beige product was washed with MeOH–H_2O (1 : 2 v/v), then acetone, and dried under vacuum

The crystal for X-ray analysis was obtained by cooling in ice the filtrate from a mixture of $Na_2[Fe(CN)_5(NO)]\cdot 2H_2O$ (1.01 g, 3.39 mmol) in H_2O (10 mL) and $MePh_3PBr$ (2.39 g, 6.69 mmol) in MeOH (10 mL)..

$(Ph_4P)_2[Fe(CN)_5(NO)]$. A solution of $Na_2[Fe(CN)_5(NO)]\cdot 2H_2O$ (0.76 g, 2.6 mmol) in 20 mL of water was stirred into a solution of Ph_4PBr (2.11 g, 5.0 mmol) in 20 mL of MeOH, forming a small amount of precipitate. The whole mixture was cooled in ice, to yield 1.24 g of pink–beige $(Ph_4P)_2[Fe(CN)_5(NO)]$, which was separated by filtration, washed with H_2O:MeOH (1 : 1 v/v) and dried under vacuum.

The crystal used for X-ray diffraction analysis was obtained by slow evaporation of the mother liquor (after removal of the initial precipitate by filtration) from a mixture of $Na_2[Fe(CN)_5(NO)]\cdot 2H_2O$ (1.5 g, 5.0 mmol) dissolved in *ca.* 38 mL of water and Ph_4PBr (2.5 g, 5.9 mmol) in *ca.* 38 mL of MeOH.

Solutions for electrospray mass spectrometry

For $(Ph_4P)_2[Fe(CN)_5(NO)]$ and $(MePh_3P)_2[Fe(CN)_5(NO)]$ approximately 10^{-4} M solutions were prepared by dissolution of the isolated solids in MeOH.

$Ag_3Fe(CN)_6]$ was prepared from a stoichiometric mixture of $K_3[Fe(CN)_6]$ and $AgNO_3$ in water: this light-sensitive solid loses its initial brick-red colour even in the dark.

10^{-3} M stock solutions of $(Ph_4P)_3[Fe(CN)_6]$ and $(MePh_3P)_3[Fe(CN)_6]$ were prepared by mixing 10 mL of ESI-grade MeOH, $Ph_4PBr\cdot 2H_2O$ or $MePh_3PI$ (0.03 mmol), and $Ag_3Fe(CN)_6]$ (0.01 mmol), and stirring overnight. The precipitate of AgX was allowed to settle, and the supernatant liquid was filtered through a 0.45 μm filter, then diluted 10-fold with MeOH.

ESMS procedures

Experiments were carried out on a Bruker Daltonics BioAPEX II FTICR mass spectrometer equipped with a 7T super conducting magnet. Three cryogenic pumps and a turbo molecular pump pumped this instrument, which has an external electrospray (Analytica) ion source.[9] The four-stage differential pumping allowed the transfer of ions from the 1 atmosphere ion source through a capillary to the cell region maintained at a pressure of 1×10^{-8} Pa.

A syringe pump was used to spray methanol or methanol–water solutions (of 1 to 10×10^{-5} M) at 60 μL h^{-1} through a spray needle with a 0.1 mm tip. The spray needle was grounded and approximately 1 cm from a nickel coated end of a quartz capillary tube. Nitrogen heated to 200 °C was used as drying gas.

Negative ion spectra were obtained with the capillary voltage maintained at 4 kV, and the outlet of the capillary into the pumped source was varied between −10 and −400 V. Positive ions were obtained with the capillary voltage maintained at −4 kV and the outlet of the capillary into the pumped source was varied between 10 and 400 V. Ions passing through the capillary entered a region with a pressure of 4×10^{-4} Pa. where they were accelerated towards a skimmer maintained at −10 V. Ions passing through the skimmer were trapped in a hexapole ion trap for a controlled period to accumulate ions. The stored ions were released as a package and, using a series of ion lenses, were guided to be trapped in the ICR cell.

Simulation of mass spectra

Spectra of all species were simulated successfully using the Bruker Xmass 5.0 package. The *m*/*z* values given in Tables 2–7 and in the text are those of the ions containing only the major isotopes (^{1}H, ^{12}C, ^{14}N, ^{56}Fe). The values were obtained by direct observation or from a simulation or both.

Crystallography

X-Ray diffraction data for $(Ph_4P)_3[Fe(CN)_6](H_2O)(BuOH)$-(hexane) and $(Me_2Ph_2P)_3[Fe(CN)_6](H_2O)_2$ were recorded at low temperature (150 K) on a Nonius Kappa-CCD diffractometer.

Table 2 Anions observed in ESI-FTICR-MS spectra of solutions of $(MePh_3P)_3[Fe(CN)_6]$ in MeOH[a]. Abbreviations: P = $MePh_3P$, Fe = $[Fe(CN)_6]$. Values of *m*/*z* are given in parentheses. The table is organised according to net charge (columns) and $[Fe(CN)_6]$ content (rows)

$P_{3n-1}Fe_n^-$	$P_{3n-2}Fe_n^{2-}$	$P_{3n-3}Fe_n^{3-}$	$P_{3n-4}Fe_n^{4-}$	$P_{3n-5}Fe_n^{5-}$
P_2Fe^- (766)				
$P_5Fe_2^-$ (1809)	$P_4Fe_2^{2-}$ (766)			
$P_8Fe_3^-$ (2853)	$P_7Fe_3^{2-}$ (1288)			
	$P_{10}Fe_4^{2-}$ (1809)	$P_9Fe_4^{3-}$ (1114)		
	$P_{13}Fe_5^{2-}$ (2331)	$P_{12}Fe_5^{3-}$ (1462)	$P_{11}Fe_5^{4-}$ (1027)[b]	
	$P_{16}Fe_6^{2-}$ (2853)	$P_{15}Fe_6^{3-}$ (1809)	$P_{14}Fe_6^{4-}$ (1288)[b,c]	
		$P_{18}Fe_7^{3-}$ (2157)	$P_{17}Fe_7^{4-}$ (1549)[b]	
		$P_{21}Fe_8^{3-}$ (2505)	$P_{20}Fe_8^{4-}$ (1809)	
			$P_{23}Fe_9^{4-}$ (2070)	
			$P_{26}Fe_{10}^{4-}$ (2331)	
			$P_{29}Fe_{11}^{4-}$ (2592)	
				$P_{31}Fe_{12}^{5-}$ (2226)
				$P_{34}Fe_{13}^{5-}$ (2435)
				$P_{37}Fe_{14}^{5-}$ (2643)

[a] Capillary voltage = −140 V, except where noted otherwise. Additional ions not fitting the pattern of this table are $PHFe^-$ (490); $P_6NaFe_3^{2-}$ (1161); $P_6KFe_3^{2-}$ (1169); $P_4HFe_2^-$ (1533); $P_{36}NaFe_{14}^{5-}$ (2593) (overlaps the signal from $P_{29}Fe_{11}^{4-}$ (2591)); $P_{36}KFe_{14}^{5-}$ (2596). [b] Capillary voltage −20 V. [c] Overlapping the signal of $P_7Fe_3^{2-}$.

Table 3 Anions with partial loss of CN^- in the ESMS spectra of solutions of $(MePh_3P)_3[Fe(CN)_6]$ in MeOH. The capillary voltage was −140 V, except for $Fe(CN)_4^-$ obtained with a capillary voltage of −200 V. Abbreviations: P = $MePh_3P$, Fe = $[Fe(CN)_6]$. Values of *m*/*z* are given in parentheses

$Fe(CN)_4^-$ (160)[a]		
$P\{[Fe(CN)_5]\}^-$ (463)		
$P_4Fe\{[Fe(CN)_5]\}^-$ (1506)		
$P_7Fe_2\{[Fe(CN)_5]\}^-$ (2550)		
	$P_9Fe_3\{[Fe(CN)_5]\}^{2-}$ (1658)	$P_{23}Fe_8\{[Fe(CN)_5]\}^{3-}$ (2752)
	$P_{11}Fe_3\{[Fe(CN)_5]\}_2^{2-}$ (2028)	
	$P_{15}Fe_5\{[Fe(CN)_5]\}^{2-}$ (2701)	

[a] Capillary voltage −200 V.

Table 4 Anions from $(Ph_4P)_3[Fe(CN)_6]$, prepared *in situ* in MeOH from Ph_4PBr and $Ag_3[Fe(CN)_6]$.[a] Abbreviations: P = Ph_4P, Fe = $[Fe(CN)_6]$. Values of *m*/*z* are given in parentheses. The table is organised according to net charge (columns) and $[Fe(CN)_6]$ content (rows)

$P_{3n-1}Fe_n^-$	$P_{3n-2}Fe_n^{2-}$	$P_{3n-3}Fe_n^{3-}$	$P_{3n-4}Fe_n^{4-}$	$P_{3n-5}Fe_n^{5-}$	$P_{3n-6}Fe_n^{6-}$	$P_{3n-7}Fe_n^{7-}$
P_2Fe^- (890)						
$P_5Fe_2^-$ (2120)						
	$P_7Fe_3^{2-}$ (1505)					
	$P_{10}Fe_4^{2-}$ (2120)	$P_9Fe_4^{3-}$ (1300)				
	$P_{13}Fe_5^{2-}$ (2734)[d]	$P_{12}Fe_5^{3-}$ (1710)	$P_{11}Fe_5^{4-}$ (1198)			
		$P_{15}Fe_6^{3-}$ (2120)	$P_{14}Fe_6^{4-}$ (1505)	$P_{13}Fe_6^{5-}$ (1136)[b]		
		$P_{18}Fe_7^{3-}$ (2529)	$P_{17}Fe_7^{4-}$ (1812)[c]	$P_{16}Fe_7^{5-}$ (1382)		
				$P_{19}Fe_8^{5-}$ (1628)		
			$P_{23}Fe_9^{4-}$ (2427)[d]	$P_{22}Fe_9^{5-}$ (1874)[c]		
				$P_{28}Fe_{11}^{5-}$ (2366)	$P_{27}Fe_{11}^{6-}$ (1915)[c]	
					$P_{33}Fe_{13}^{6-}$ (2324)[b]	$P_{29}Fe_{12}^{7-}$ (1768)[b]
						$P_{32}Fe_{13}^{7-}$ (1944)[b,c]
						$P_{38}Fe_{15}^{7-}$ (2295)[b]

[a] Capillary voltage −142 V, except as noted otherwise. Other ions are $P[Fe(CN)_5]^-$ (525); $HPFe^-$ (552); $NaPFe^-$ (574); $KPFe^-$ (590); $NaP_3Fe_2^{2-}$ (732); $KP_3Fe_2^{2-}$ (740); $P_4NaFe_2^-$ (1803); $KP_{26}Fe_{11}^{6-}$ (1865);[b] $NaP_{10}Fe_5^{4-}$ (1119);[b] $KP_{10}Fe_5^{4-}$ (1123);[b] $KP_{13}Fe_6^{4-}$ (1430);[b] $KP_{18}Fe_8^{5-}$ (1568);[b] $KP_{29}Fe_{12}^{6-}$ (2070).[b] [b] Capillary voltage −100 V. [c] Could not be observed: these signals would overlap with the stronger signals of $P_5Fe_2^-$, $P_{10}Fe_4^{2-}$ and $P_{15}Fe_6^{3-}$. [d] Plus $P_{26}Fe_{10}^{4-}$ (2734)?; overlaps stronger spectrum of $P_{13}Fe_5^{2-}$.

The SHELXTL-NT V6.1 program package was used to solve the structures by direct methods. Subsequent difference Fourier syntheses allowed the remaining atoms to be located. The hydrogen atoms were calculated geometrically and were riding on their respective carbon atoms. The phenyl rings were constrained to be rigid groups of hexagonal symmetry.

Data for $(MePh_3P)_2[Fe(CN)_5(NO)](H_2O)_2$ and $(Ph_4P)_2[Fe(CN)_5(NO)]$ were recorded at 294 K on an Enraf-Nonius CAD4 diffractometer. Structures were solved by direct methods (SIR92) and refined using RAELS.[10] Phenyl rings were modelled as rigid groups of *mm*2 symmetry. Hydrogen atoms were included in calculated positions. Phenyl rings were refined using TLX thermal parameters, and the remaining non-hydrogen atoms were refined anisotropically.

In $(Ph_4P)_3[Fe(CN)_6](H_2O)(BuOH)(hexane)$ the asymmetric unit contains half the anion, located on a centre of inversion, and 1.5 cations, one in a general position and one on a two-fold axis. There are three different solvent molecules. The water oxygen and the central bond of the hexane are located on two-fold axes. The butanol was modelled with disorder about another two-fold axis. Constraints were applied to the butanol and hexane solvents to maintain sensible geometry. All non-hydrogen atoms of the anion and cations, along with the water oxygen atom were refined anisotropically. The non-hydrogen atoms of the butanol and hexane were refined isotropically.

$(Me_2Ph_2P)_3[Fe(CN)_6](H_2O)_2$ contains two crystallographically different anions, with Fe atoms located on two-fold axes. The three independent cations and the two solvent water

Table 5 Negative ions from $(MePh_3P)_2[Fe(CN)_5(NO)]$ in MeOH. Abbreviations: P = $MePh_3P$, Fe = $[Fe(CN)_5(NO)]$. Values of *m*/*z* are given in parentheses

$P_{2n-1}Fe_n^-$
PFe^- (493)[a]
$P_3Fe_2^-$ (1263)[a]
$P_5Fe_3^-$ (2033)[b]
$P_7Fe_4^-$ (2804)[b]

[a] At both −20 and −150 V. [b] At −150 V only.

Table 6 Negative ions[a] from $(Ph_4P)_2[Fe(CN)_5(NO)]$ in MeOH. Abbreviations: P = Ph_4P, Fe = $[Fe(CN)_5(NO)]$. Values of *m*/*z* are given in parentheses

$P_{2n-1}Fe_n^-$	$P_{2n-2}Fe_n^{2-}$
PFe^- (555)[b]	
$P_3Fe_2^-$ (1449)	
	$P_4Fe_3^{2-}$ (1002)[d]
$P_5Fe_3^-$ (2343)[c]	$P_6Fe_4^{2-}$ (1449)[e]
$P_7Fe_4^-$ (3238)[e]	$P_8Fe_5^{2-}$ (1896)[e]
	$P_{10}Fe_6^{2-}$ (2343)[e]

[a] All species observed at capillary voltage = −150 to +1 V, unless noted otherwise. [b] CID gives $H[Fe(CN)_5(NO)]^-$ (217). [c] Not at capillary voltage = +1 V. [d] Not at capillary voltage < −100 V. [e] At capillary voltages ≤ −100 V.

Table 7 Positive ions from $(Ph_4P)_2[Fe(CN)_5(NO)]$ in MeOH. Abbreviations: P = Ph_4P, Fe = $[Fe(CN)_5(NO)]$. Values of *m*/*z* are given in parentheses

$P_{2n+1}Fe_n^+$	$P_{2n+2}Fe_n^{2+}$
P^+ (339)	
P_3Fe^+ (1233)	
$P_5Fe_2^+$ (2128)	
$P_7Fe_3^+$ (3022)	
$P_9Fe_4^+$ (3916)	
$P_{11}Fe_5^+$ (4810)	$P_{12}Fe_5^{2+}$ (2575)
	$P_{14}Fe_6^{2+}$ (3022)

molecules are located in general positions. All non-hydrogen atoms were refined anisotropically.

In $(MePh_3P)_2[Fe(CN)_5(NO)](H_2O)_2$, the Fe atom is located on a centre of inversion, and so the NO ligand and its centrosymmetrically related CN are disordered. A combined scattering curve was used for each of the atoms of these ligands.

Crystal data for the four compounds are given in Table 1

CCDC reference numbers 200409–200412.

See http://www.rsc.org/suppdata/dt/b2/b212488b/ for crystallographic data in CIF or other electronic format.

Density functional calculations

The intermolecular potentials for CH_4 with NC^-, CH_4 with $NCCH_3$, C_6H_6 with NC^- and C_6H_6 with $[NCCuCN]^-$ were calculated as the energy differences (pair − components) as a function of separation for the linear geometries C–H ··· NC^- and C–H ··· $NCCH_3$: results not presented revealed that these linear geometries were most favourable, as expected. Energies were calculated with the program DMol[3],[11] using numerical basis sets[12] evaluated over a very large grid, thereby avoiding basis set superposition uncertainties.[13] Selection of the density functional is crucial,[14] and is founded on extensive calculations for well-known intermolecular potentials, using intermolecular distance and energy as evaluation criteria.[15] Intermolecular energies are slightly underestimated by the Perdew–Wang nonlocal functional[16] (functional p91 in DMol[3]) and slightly overestimated by the Perdew–Wang local functional,[17] (functional pwc in DMol[3]) depending on chemical functionality. For the present systems the p91 results are considered to be more accurate and are reported.

Results and interpretations

Electrospray mass spectra of the cations Ph_4P^+ or $MePh_3P^+$ associated with the anions $[Fe(CN)_6]^{3-}$ or $[Fe(CN)_5(NO)]^{2-}$

Methanol solutions of these compounds were investigated by ESMS. A representative spectrum is shown in Fig. 1. All peaks could be assigned unambiguously, from accurate mass measurements and simulations. Contaminating alkali metal cations occur in some of the observed species.

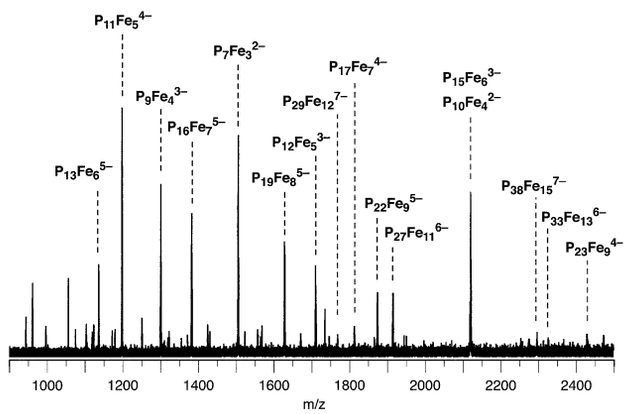

Fig. 1 Part of the negative ion spectrum of a solution of $(Ph_4P^+)_3[Fe(CN)_6^{3-}]$ in methanol. The capillary voltage was −100 V. Significant peaks are identified.

The principal species of interest are tabulated in Tables 2–7. Throughout these tables the abbreviation P is used for the phosphonium cation Ph_4P^+ or $MePh_3P^+$, and Fe is used for the cyanoferrate anion $[Fe(CN)_6]^{3-}$ or $[Fe(CN)_5(NO)]^{2-}$. Information about the capillary voltages required to generate the species is also contained in the tables.

Ions from $(MePh_3P)_3[Fe(CN)_6]$ in MeOH

Table 2 lists the anions with the general composition $[(MePh_3P)_{3n-x}\{Fe(CN)_6\}_n]^{x-}$ obtained from a solution of $(MePh_3P)_3[Fe(CN)_6]$ produced *in situ* in MeOH. In addition there were some ions with partial loss of cyanide, containing the $[Fe(CN)_5]$ moiety, listed in Table 3: higher capillary voltages were not generally needed to fragment $[Fe(CN)_6]$. Further fragmentation to $[Fe(CN)_4]^-$ at higher voltages is noteworthy. It is possible that the process $MePh_3P^+ + [NC–Fe(CN)_5]^{3-} \longrightarrow [Fe(CN)_5]^{2-} + MeCN + Ph_3P$ is responsible for this elimination of CN.

Only a few positive ions were obtained from this solution of $(MePh_3P)_3[Fe(CN)_6]$ in MeOH (capillary at +100 V): $MePh_3P^+$ (277); $[(MePh_3P)_3K\{Fe(CN)_6\}]^+$ (1082); $[(MePh_3P)_4\{Fe(CN)_6\}]^+ \rightleftharpoons [(MePh_3P)_8\{Fe(CN)_6\}_2]^{2+}$ (1320); and $[(MePh_3P)_{11}\{Fe(CN)_6\}_3]^{2+}$ (1842).

The most prominent feature of the negative-ion ESMS of $(MePh_3P)_3[Fe(CN)_6]$ in MeOH is the occurrence of extended series of aggregates containing only $MePh_3P^+$ and $[Fe(CN)_6]^{3-}$, with net charges ranging from 1– to 5–.

Ions from $(Ph_4P)_3[Fe(CN)_6]$ in MeOH

Table 4 lists the negative ions observed from a solution of $(Ph_4P)_3[Fe(CN)_6]$ in MeOH, organised in the same fashion as Table 2 (see also Fig. 1). In this case the series of aggregates $[(Ph_4P)_{3n-x}\{Fe(CN)_6\}_n]^{x-}$ extends to $x = 7$. In contrast only three positive ions were observed: PPh_4^+, P_4Fe^+ and $P_7Fe_2^+$.

Ions from $(MePh_3P)_2[Fe(CN)_5(NO)]$ in MeOH

The few negative ions are listed in Table 5. Species with loss of one NO were also observed. The positive ions (capillary voltage = −4 V) observed were P^+, (277); P_3Fe^+ (1047); $P_5Fe_2^+$ (1817) (abbreviations: P = $MePh_3P$, Fe = $[Fe(CN)_5(NO)]$).

Ions from $(Ph_4P)_2[Fe(CN)_5(NO)]$ in MeOH

This solution yielded larger ranges of negative ions (Table 6) and positive ions (Table 7) than did $(MePh_3P)_2[Fe(CN)_5(NO)]$ in MeOH. Other significant negative ions were $P_2NaFe_2^-$ (1133) and $P_2KFe_2^-$ (1149). All of the Fe-containing positive ions in Table 7 except $P_9Fe_4^+$ and possibly $P_{11}Fe_5^+$ showed a clear signal from loss of one NO, *e.g.* $[P_5Fe_2 - NO]^+$ (2098) and $[P_{12}Fe_5 - NO]^{2+}$ (2560).

General properties of the aggregates

Large aggregates can be observed: the largest is comprised of 53 component cations and anions, $[(Ph_4P)_{38}\{Fe(CN)_6\}_{15}]^{7-}$. These are nanoclusters of molecular ions: the models described below show that the largest aggregate has a diameter of 4–5 nm, and intermediate clusters have diameters of *ca*. 3 nm. The patterns of stoichiometry (cation/anion ratios) are evident in the Tables. The ratios of phosphonium cations to anions in the anionic aggregates are relatively small (1 for $[Fe(CN)_5(NO)]^{2-}$ and 2 for $[Fe(CN)_6]^{3-}$) only in the smallest aggregates, but in the larger aggregates there tends to be about 2.5 cations per $[Fe(CN)_6]^{3-}$. Concomitant with this the charge densities (charge per component) in the larger aggregates tend towards a value in the range −0.1 to −0.2 with increasing size. For example, the charge per component ion in $[(Ph_4P)_{38}\{Fe(CN)_6\}_{15}]^{7-}$ is −0.13. No methanol solvent was included in the ion aggregates, and we believe that this is related to the low charge densities within them.

Further significant questions about these aggregates concern their structures and structural principles, and their cohesive energies. We have approached the questions of structure through examination of the associations of the same ions (Ph_4P^+, $MePh_3P^+$, $[Fe(CN)_6]^{3-}$, $[Fe(CN)_5(NO)]^{2-}$) in molecular crystals, choosing crystals where the cation to anion ratio spans the range observed in the gaseous aggregates. These results are presented next.

Crystal packing for the cations Ph_4P^+, $MePh_3P^+$ and $Me_2Ph_2P^+$ associated with anions $[Fe(CN)_6]^{3-}$ and $[Fe(CN)_5(NO)]^{2-}$

The crystals $(Ph_4P)_3[Fe(CN)_6](H_2O)(BuOH)(hexane)$, $(Me_2Ph_2P)_3[Fe(CN)_6](H_2O)_2$, $(MePh_3P)_2[Fe(CN)_5(NO)](H_2O)_2$ and $(Ph_4P)_2[Fe(CN)_5(NO)]$ were obtained as described in the Experimental section. To date, we have not been able to crystallise $(MePh_3P)_3[Fe(CN)_6]$. Two of these crystals have three cations per anion, and two have two cations per anion, and are thereby able to reveal any packing differences due to cation/anion volume proportions, spanning the range of these proportions occurring in the gas phase. These four crystals show four different but similar crystal packing arrangements[18] and so provide four perspectives on the principles of molecular packing for these cations and anions.

The packing types are illustrated in Fig. 2. Also shown in Fig. 2 are the hydrogen bonds involving solvent that occur in three of the crystals. The solvent always forms CN ··· HOH ··· NC hydrogen bonds, intramolecular in $(MePh_3P)_2[Fe(CN)_5(NO)](H_2O)_2$ (Fig. 2(c)) and intermolecular in $(Ph_4P)_3[Fe(CN)_6](H_2O)(BuOH)(hexane)$ and $(Me_2Ph_2P)_3[Fe(CN)_6](H_2O)_2$: no solvent ··· solvent hydrogen bonds occur. There is CN/NO disorder at two *trans* coordination positions of $[Fe(CN)_5(NO)]^{2-}$ in $(MePh_3P)_2[Fe(CN)_5(NO)](H_2O)_2$.

In each of the four structures the anions are arrayed in approximately cubic (primitive or body-centred) fashion, with no significant association of the anions other than through the hydrogen bonds portrayed in Fig. 2. Distances between the anion centres are listed in the caption to Fig. 2.

It is well-established that the cations Ph_4P^+ and $MePh_3P^+$ associate through phenyl ··· phenyl interactions of the offset face-to-face (OFF) or edge-to-face (EF) types, and that these motifs can operate in concert to form multiple phenyl embraces of the types 6PE, P4PE and O4PE, which can further associate to form chains and nets.[8] However, these multiple phenyl embraces are very poorly developed in the crystals reported here, and they are not a significant factor in the crystal packing.

What then are the interactions that control the lattice packing in these crystals? The non-directional cation ··· anion electrostatic energies clearly favour the general non-segregation of homo-charged ions, and these energies are discussed further below. However, there is also very clear evidence of a motif that dominates the crystal packing in all four structures, namely charge-assisted C–H ··· N hydrogen bonding between the phenyl and methyl hydrogen atoms on cations and the terminal N of coordinated cyanide. Since there will be some partial negative charge on coordinated cyanide ligands, and because many of the C–H ··· N connections are observed to approach linearity, we regard them as hydrogen bonds. In the two crystals containing $[Fe(CN)_5(NO)]^{2-}$, C–H ··· O hydrogen bonds occur between the cations and the terminal O(N) atom. Identification of these C–H ··· N and C–H ··· O interactions uses H–N and H–O distance criteria derived from the relevant intermolecular energy potentials (described below), and includes all H–N and H–O distances ranging up to 3.0 Å, and some slightly longer distances where the C–H ··· N/C–H ··· O angles approach 180°.

Fig. 3 shows details of these hydrogen bonds for three of the four crystals. In all cases the cations form these interactions with more than one anion and the anion with more than one cation. The hexagonal prismatic set of twelve Ph_4P^+ cations around $[Fe(CN)_6]^{3-}$ in $(Ph_4P)_3[Fe(CN)_6](H_2O)(BuOH)(hexane)$ uses 16 phenyl rings in 16 C–H ··· N interactions (Fig. 3(a)). The net of C–H ··· N and C–H ··· O interactions in $(MePh_3P)_2[Fe(CN)_5(NO)](H_2O)_2$ is shown in Fig. 3(b). A further feature is the general occurrence of chelating hydrogen bonds, in which *ortho* C–H groups of a phenyl ring interact with the same cyanide N atom, or *cis* $(CN)_2$ ligands, or *cis* (CN)(NO) ligands. Two phenyl rings of the same cation can also form these chelating hydrogen bonds. The chelating features are illustrated in a section of the structure of $(Ph_4P)_2[Fe(CN)_5(NO)]$ portrayed in Fig. 3(c).

Each of the four crystals contains a fairly dense web of these hydrogen bonds, and they are clearly the motifs that have determined the details of the crystal packing. While the locations of the anions and cations are generally consistent with ion electrostatics, the rotational orientations of both the spikey anions and the globular cations are determined by the net of charge assisted C–H ··· N (and C–H ··· O) hydrogen bonds. The principal metrical characteristics of these hydrogen bonds are: (1) the H–N/O distances range from 2.4 to *ca*. 3.2 Å; (2) the C–H–N/O angles range from *ca*. 130 to 180°; (3) an approach to coplanarity of N/O with the phenyl ring; (4) the occurrence of four or five interactions at each N/O atom, and a concomitant approach to approximate orthogonality at N/O, as idealised in the diagram below; (5) chelation, involving *ortho* $(CH)_2$ of one phenyl ring and/or CH on different phenyl rings of a cation.

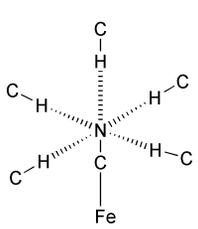

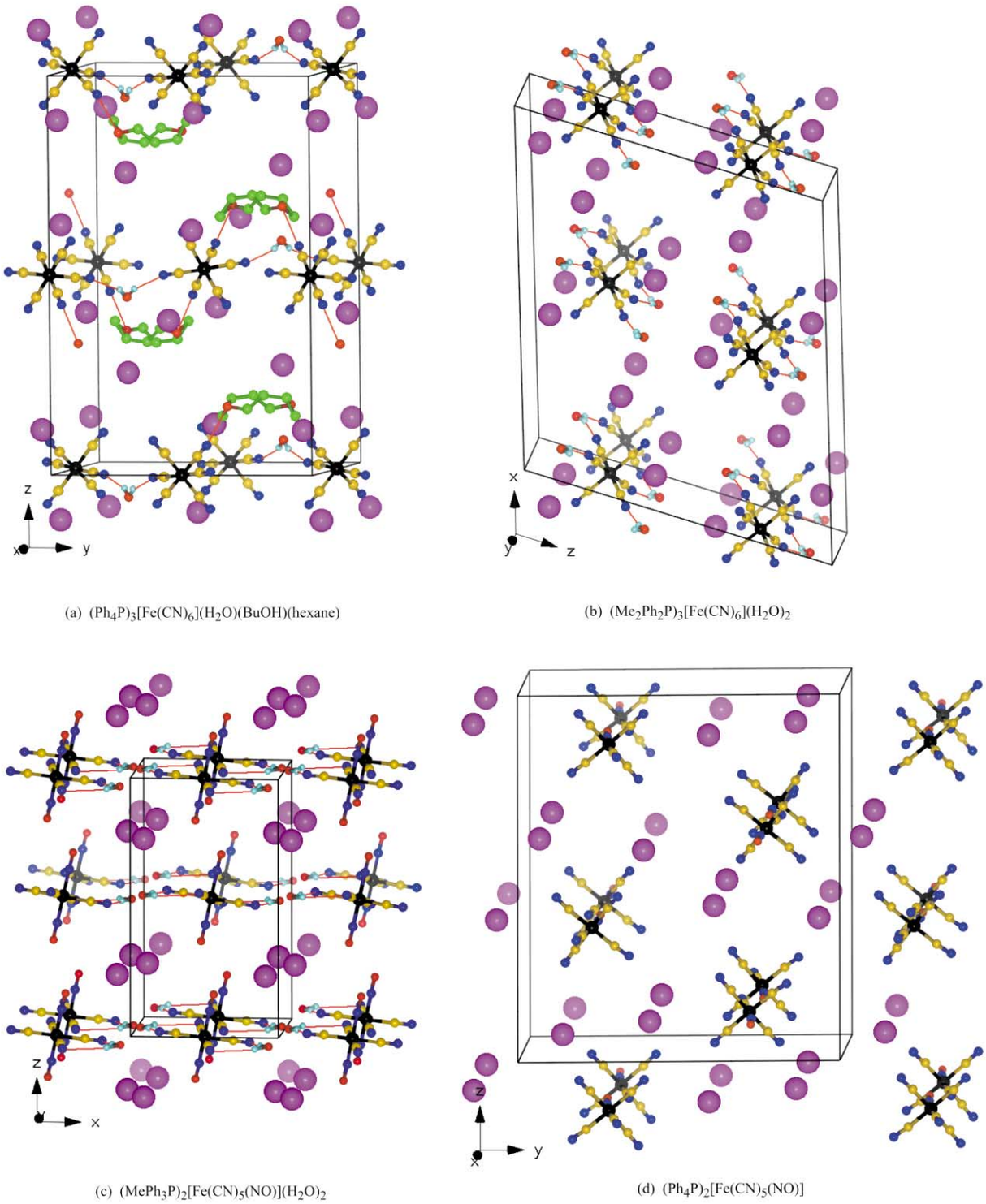

(a) $(Ph_4P)_3[Fe(CN)_6](H_2O)(BuOH)(hexane)$

(b) $(Me_2Ph_2P)_3[Fe(CN)_6](H_2O)_2$

(c) $(MePh_3P)_2[Fe(CN)_5(NO)](H_2O)_2$

(d) $(Ph_4P)_2[Fe(CN)_5(NO)]$

Fig. 2 The overall lattice packing arrangements in (a) $(Ph_4P)_3[Fe(CN)_6](H_2O)(BuOH)(hexane)$, (b) $(Me_2Ph_2P)_3[Fe(CN)_6](H_2O)_2$, (c) $(MePh_3P)_2$-$[Fe(CN)_5(NO)](H_2O)_2$ and (d) $(Ph_4P)_2[Fe(CN)_5(NO)]$. The cations are shown as the P (magenta) positions only, with phenyl and methyl groups omitted; Fe black, cyanide C yellow, N blue, O red, H cyan; hydrogen bonds are drawn as red rods. In (a), space group *Pccn*, the $[Fe(CN)_6]^{3-}$ are linked by hydrogen bonding water molecules, and are hydrogen bonded to disordered butanol molecules (C bright green): the anion separations (Fe ··· Fe) are 11.9, 15.4, 15.9 Å. In (b), projected along the shortest axis (9.1 Å) in space group *P*2/*c*, the anions are linked by CN ··· HOH ··· NC hydrogen bonds: other anion separations (Fe ··· Fe) are 10.9, 12.6, 14.3 Å. In (c), space group $P2_1/c$, the disordered *trans* CN/NO ligands in $[Fe(CN)_5(NO)]^{2-}$ are drawn as NO: the water molecules hydrogen bond between *cis* ordered CN ligands in the anion. The shorter Fe ··· Fe distances are 9.8, 10.5, 12.0 Å. In (d) (space group $P2_1/c$) there are columns of anions (with no specific interaction between them) surrounded by cations. The shorter Fe ··· Fe distances are 9.0, 11.8, 12.2, 12.4, 12.8, 13.2 Å.

These are the metrical patterns of association. However, energy rather than geometry is the determining property, and an understanding of the association of phenylated cations and cyanometallate anions requires information about the energies involved. In the absence of experimental data we have calculated these energies and some energy–distance potentials, as described next.

Energies of association in the gas-phase aggregates

Electrostatic energies will clearly play a major role in the aggregation of Ph_4P^+, $MePh_3P^+$ or $Me_2Ph_2P^+$ with $[Fe(CN)_6]^{3-}$ or $[Fe(CN)_5(NO)]^{2-}$. The general dispersal of oppositely charged ions in the four crystal structures (Fig. 2) attests to the influence of electrostatic energies. The crystal structures also make it evi-

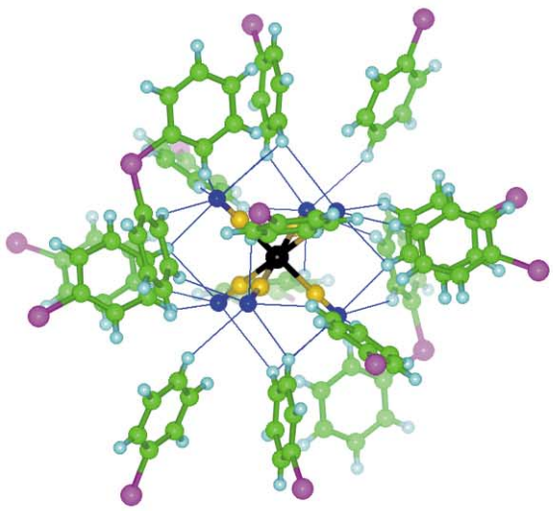

(a) $(Ph_4P)_3[Fe(CN)_6](H_2O)(BuOH)(hexane)$

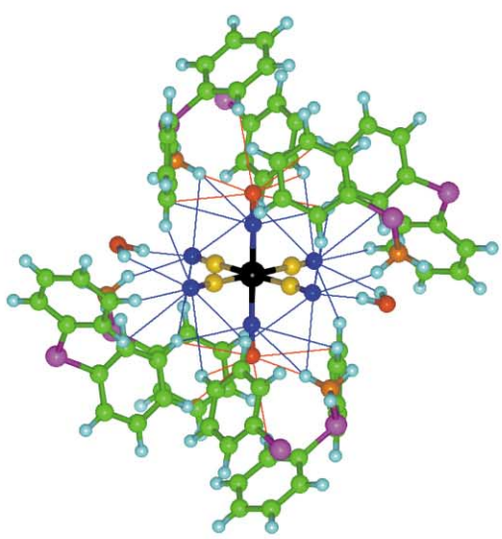

(b) $(MePh_3P)_2[Fe(CN)_5(NO)](H_2O)_2$

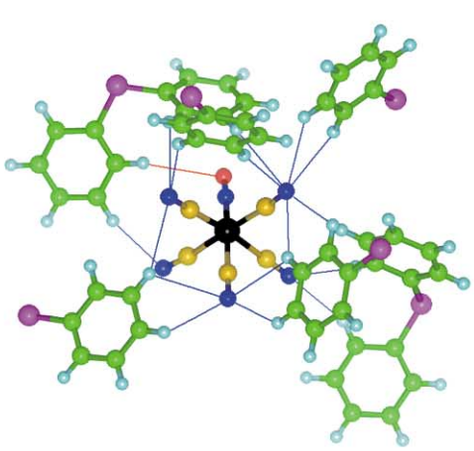

(c) $(Ph_4P)_2[Fe(CN)_5(NO)]$

Fig. 3 Details of the C–H ··· N and C–H ··· O local motifs. (a) The immediate surroundings of $[Fe(CN)_6]^{3-}$ in $(Ph_4P)_3[Fe(CN)_6](H_2O)$-(BuOH)(hexane): uninvolved phenyl rings, and the two hydrogen bonded water molecules, are omitted. The blue rods identify the 16 C–H ··· N interactions (H ··· N ≤ 3.2 Å) with $[Fe(CN)_6]^{3-}$, involving 16 phenyl rings from 14 cations. (b) The well formed C–H ··· N(NC) (blue) and C–H ··· O(ON) (red) interactions in $(MePh_3P)_2[Fe(CN)_5$-$(NO)](H_2O)_2$. (c) Part of the surroundings of $[Fe(CN)_6]^{3-}$ in $(Ph_4P)_2[Fe(CN)_5(NO)]$, selected to emphasise the seven sets of chelating hydrogen bonds involving ortho-CH of phenyl groups.

dent that cation–anion C–H ··· N hydrogen bonding is likely to occur in the gas phase aggregates, and therefore information about the magnitudes of these hydrogen bond energies is valuable when attempting to understand the energy balances in the ion aggregates.

The potential surface of the C–H ··· N motif has been investigated using our density functional method applied to the hydrogen bonding of the four model systems CH_4 with $NCCH_3$, CH_4 with NC^-, C_6H_6 with $[NCCuCN]^-$, and C_6H_6 with NC^-. The acceptors in these systems bracket the negative charge density likely to occur in a cyanide ligand of $[Fe(CN)_6]^{3-}$ or $[Fe(CN)_5(NO)]^{2-}$. The potentials are presented in Fig. 4. As expected, the charge enhancement of the hydrogen bond energy from CH_4 to neutral acetonitrile and then to CN^- is evident in the increased depth and shortened distance of the potential well. Similarly, C_6H_6 is a stronger hydrogen bond donor than CH_4, as seen in the C_6H_6 ··· CN^- combination. The C_6H_6 ··· $[NCCuCN]^-$ potential provides the best approach to the acceptor charge density (*ca.* −0.5 per CN) in the cyanoferrate anions, but the actual potential is expected to be stabilised further by the enhanced positive density on the phenyl hydrogen atoms in the cations. Superimposed on the calculated potentials in Fig. 4 is the distribution of H ··· N distances in the crystal structures reported here. All of the calculated potential minima occur at slightly shorter H ··· N distances than observed in the crystals, as expected because the calculation involves a single pair devoid of the competing stabilisation from the full surrounds in the crystal, but energies at the observed distances can be read from these potentials. Therefore we conclude that the stabilisation energy of the actual (phenyl)-C–H ··· $NCFe(CN)_{4,5}$ hydrogen bonds is *ca.* 4 kcal mol^{-1} in the H ··· N distance range 2.4–3 Å. With of the order of 15 such hydrogen bonds per anionic complex, an estimate of its hydrogen bonding energy with surrounding cations is *ca.* 60 kcal mol^{-1}.

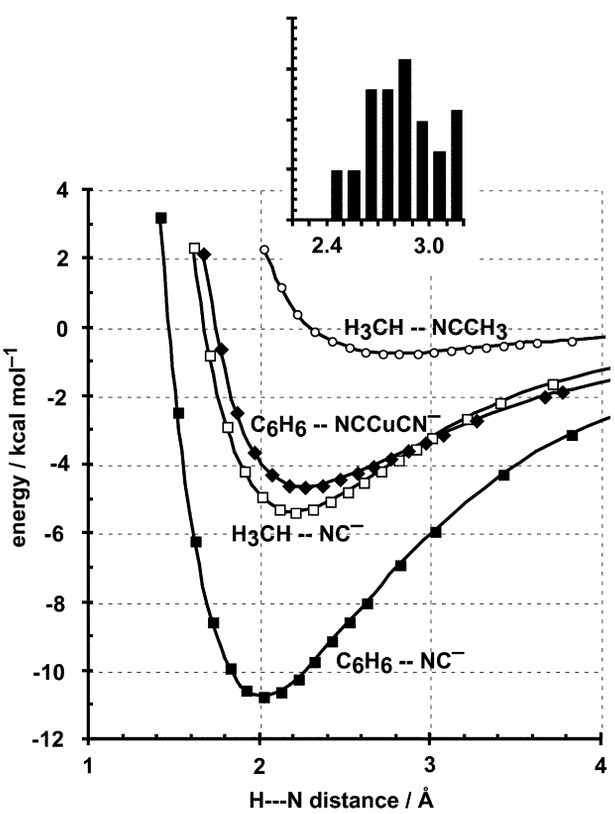

Fig. 4 Calculated intermolecular potentials for the interactions CH_4 ··· $NCCH_3$ (○), CH_4 ··· NC^- (□), C_6H_6 ··· $[NCCuCN]^-$ (◆) and C_6H_6 ··· NC^- (■), all with linear C–H ··· N. The inset shows the histogram of H ··· N distances observed in the four crystal structures, on the same distance axis as the intermolecular potentials.

Electrostatic energies for polyatomic ions can be estimated (in the absence of accurate calculations) *via* Coulomb's law for net charges at the ion centres, modulated by the permittivity ε of the through-ion interactions. A common approximation for the magnitude of this permittivity is $\varepsilon = d$ (in Å). In this way the electrostatic energy (kcal mol^{-1}) between $[Fe(CN)_5(NO)]^{2-}$ and Ph_4P^+ is estimated to be −15 (−99 for $\varepsilon = 1$) at 6.5 Å (the closest observed separation) and −6.5 (−64) at 10 Å. Similarly, the electrostatic energy for a pair of $[Fe(CN)_5(NO)]^{2-}$ at Fe–Fe = 9 Å is +16 (+143 for $\varepsilon = 1$) kcal mol^{-1}, and for a pair of $[Fe(CN)_6]^{3-}$ at Fe–Fe = 10 Å is +29 (+290) kcal mol^{-1}, while for Ph_4P^+ pairs at the observed separations (6–8 Å) the electrostatic energy (kcal mol^{-1}) is estimated to range from +9 to +5 (+54 to +40 for $\varepsilon = 1$). While these energy estimates are crude (largely due to uncertainty about the permittivity of aggregates of polyatomic ions), it seems clear that they support a general concept of energy balance in which the net electrostatic energies and the net hydrogen bonding energies in these ion-aggregates are of similar magnitude. Multiple phenyl embraces are not energetically competitive in this context.

Probable structures for the ion aggregates in the gas phase

From all of the preceding results a model emerges for the observed ion aggregates in the gas phase. Electrostatic influences generate arrays of ions surrounded by charge opposites to the extent permitted by the cationic excess, while local contact between ions is influenced by the formation of C–H ··· N hydrogen bonds. The solvent-based hydrogen bonds of three of the crystals are absent from the gas phase aggregates. Fluid structures are expected for the gaseous aggregates, and we tested this expectation using a simple model including coulombic energies between ions as monopoles, with an artificial repulsive potential to keep oppositely charged ions at the appropriate distances: energy minimisations yielded numerous structures and interconversions for the aggregates.

The observed gaseous aggregates can be large. Fig. 5 shows postulated models (H omitted) for $[(Ph_4P^+)_{19}\{[Fe(CN)_6]^{3-}\}_8]^{5-}$ and $[(Ph_4P^+)_{38}\{[Fe(CN)_6]^{3-}\}_{15}]^{7-}$, generated as globular fragments of the crystal structure. Some of the $[Fe(CN)_6]^{3-}$ ions protrude to the surface, which is mainly comprised of Ph_4P^+ ions. The diameter of the $[(Ph_4P^+)_{19}\{[Fe(CN)_6]^{3-}\}_8]^{5-}$ model is 3–4 nm, while that of $[(Ph_4P^+)_{38}\{[Fe(CN)_6]^{3-}\}_{15}]^{7-}$ is 4–5 nm.

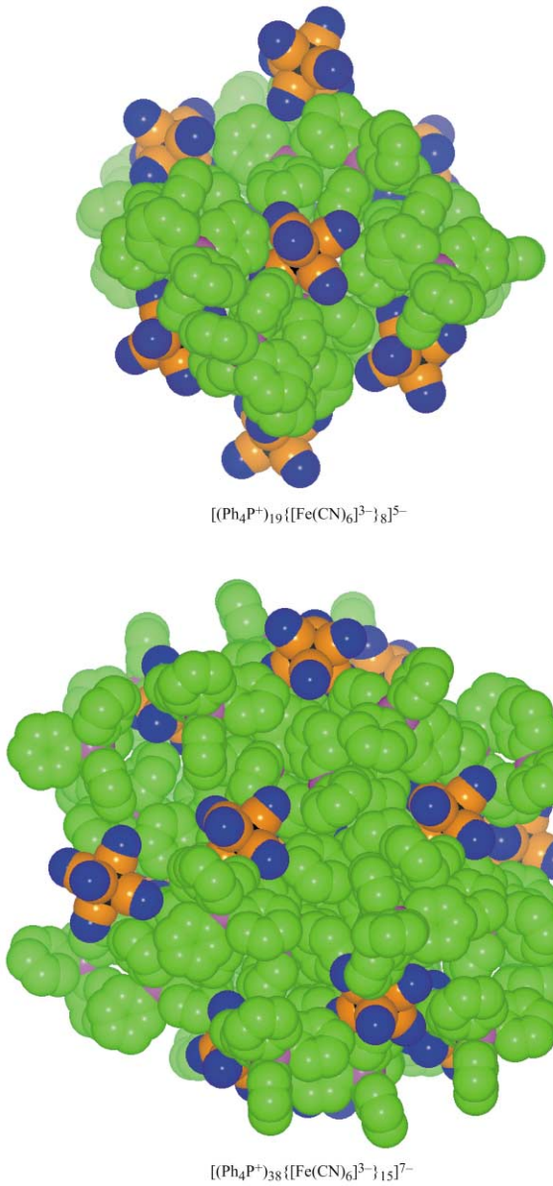

Fig. 5 Postulated models for the observed aggregates $[(Ph_4P^+)_{19}\{[Fe(CN)_6]^{3-}\}_8]^{5-}$ and $[(Ph_4P^+)_{38}\{[Fe(CN)_6]^{3-}\}_{15}]^{7-}$, generated as fragments of the crystal structure (H atoms not shown, cyano carbon orange), and represented on the same scale. The diameters are 3–4 nm and 4–5 nm, respectively.

Conclusions

The association of phenylphosphonium cations and penta- or hexa-cyanoferrate anions is readily achieved during the electrospray process from methanol. Negatively and positively charged aggregates are observed, with patterns of composition and charge density.

The structural principles derived from analysis of the packing of these ions in four relevant crystal structures are that the arrangements of component cations and anions in these aggregates, while fluid, will maximise the surrounding of the cyanoferrate anions by the more numerous phenylphosphonium cations, with the formation of many local C–H ··· N hydrogen bonds, and without multiple phenyl embraces. Inclusion of hydrogen bonding solvent molecules is minimal in the crystals and absent in the gas phase aggregates, indicating that these hydrogen bonds are uncompetitive in the milieu of phenylphosphonium cations and cyanometallate anions.

Given these structural principles, it is conceivable that larger aggregates with almost the stoichiometric ratio of component cations and anions could form: for instance, aggregates such as $[(MePh_3P^+)_{33}\{[Fe(CN)_6]^{3-}\}_{12}]^{3-}$, $[(MePh_3P^+)_{34}\{[Fe(CN)_6]^{3-}\}_{12}]^{2-}$ and $[(MePh_3P^+)_{35}\{[Fe(CN)_6]^{3-}\}_{12}]^{-}$ would be structurally acceptable (with compositions similar to ions observed, Table 2), but such species could not be detected in the electrospray experiments because the *m*/*z* values exceed our instrumental capability. For the larger aggregates there are tendencies towards compositions that yield an overall charge density of *ca.* −0.15 per component species.

An important finding from analyses of the relevant crystal structures is the ubiquity of hydrogen bonds between the phenyl groups of the cations and the partially negative CN (and NO) ligands of the anions. Potentials for these hydrogen bonds have been developed, with the general conclusion that these charge-assisted C–H ··· N hydrogen bonds have energies of *ca.* 4 kcal mol^{-1}, similar to that of O–H ··· O in water.[19] It is estimated that the total energy contribution of these hydrogen bonds matches the magnitudes of the electrostatic energies in these aggregates, being augmented by electrostatic energies derived from heterocharged species and diminished by those between homocharged ions. Similar hydrogen bonds to coordinated cyanide have been reported.[20] We predict that other crystals containing anionic cyanometallate complexes and phenylated cations will also be packed according to the formation of these hydrogen bonds.

Acknowledgements

This research is funded by the Australian Research Council and the University of New South Wales. P. A. W. D., Visiting Professor at UNSW, thanks the University of Western Ontario for a sabbatical leave.

References

1 T. Iwamoto, S.-I. Nishikiori and T. Kitazawa, *Supramol. Chem.*, 1995, **6**, 179–186; T. Iwamoto, in *Comprehensive Supramolecular Chemistry*, ed. D. D. MacNicol, F. Toda and R. Bishop, Pergamon, Oxford, 1996, pp. 643–690; K. R. Dunbar and R. A. Heintz, *Prog. Inorg. Chem.*, 1997, **45**, 283–391.

2 W. R. Entley and G. S. Girolami, *Science*, 1995, **268**, 397–400; J. Larionova, M. Gross, M. J. Pilkington, H. Andres, H. Stoeckli-Evans, H. U. Gudel and S. Decurtins, *Angew. Chem., Int. Ed.*, 2000, **39**, 1605–1609; J. L. Sokol, M. P. Shores and J. R. Long, *Angew. Chem., Int. Ed.*, 2001, **40**, 236–239; J. S. Miller and J. L. Manson, *Acc. Chem. Res.*, 2001, **34**, 563–570.

3 J. T. Culp, J.-H. Park, D. Stratakis, M. W. Meisel and D. R. Talham, *J. Am. Chem. Soc.*, 2002, **124**, 10083–10090.

4 Y. Zhao, M. Hong, W. Su, R. Cao, Z. Zhou and A. S. C. Chan, *J. Chem. Soc., Dalton Trans.*, 2000, 1685–1686.

5 S. J. Gaskell, *J. Mass Spectrom.*, 1997, **32**, 677–688; W. Henderson, B. K. Nicholson and L. J. McCaffrey, *Polyhedron*, 1998, **17**, 4291–4313.

6 C. Hasselgren, K. J. Fisher, S. Jagner and I. G. Dance, *Chem. Eur. J.*, 2000, **6**, 3671–3678.

7 X.-G. Zhang, H.-Y. Li, C.-S. Ma, X.-Y. Wang, J.-L. Bai, G.-Z. He and N.-O. Lou, *Chem. Phys. Lett.*, 1997, **274**, 115; M. C. B. Moraes, J. G. A. B. Neto and C. L. Do Lago, *Int. J. Mass Spectrom.*, 2000, **198**, 121–132; I. Dance, P. A. W. Dean, K. Fisher and H. H. Harris, *Inorg. Chem.*, 2002, **41**, 3560–3569.

8 I. Dance and M. Scudder, *Chem. Eur. J.*, 1996, **2**, 481–486; I. Dance and M. Scudder, *J. Chem. Soc., Dalton Trans.*, 1996, 3755–3769; C. Hasselgren, P. A. W. Dean, M. L. Scudder, D. C. Craig and I. G. Dance, *J. Chem. Soc., Dalton Trans.*, 1997, 2019–2027; M. Scudder and I. Dance, *J. Chem. Soc., Dalton Trans.*, 1998, 329–344; C. Horn, I. G. Dance, D. Craig, M. L. Scudder and G. A. Bowmaker, *J. Am. Chem. Soc.*, 1998, **120**, 10549–10550; M. Scudder and I. Dance, *J. Chem. Soc., Dalton Trans.*, 1998, 3155–3166; M. Scudder and I. Dance, *J. Chem. Soc., Dalton Trans.*, 1998, 3167–3176; G. A. Bowmaker, P. D. W. Boyd, C. E. F. Rickard, M. L. Scudder and I. G. Dance, *Inorg. Chem.*, 1999, **38**, 5476–5477; T. Steiner, *New J. Chem.*, 2000, **24**, 137–142.

9 R. L. C. Lau, J. Jiang, D. K. P. Ng and T.-W. D. Chan, *J. Am. Soc. Mass. Spectrom.*, 1997, **8**, 161.

10 A. D. Rae, RAELS92, a Comprehensive Constrained Least Squares Refinement Program, Australian National University, Canberra, Australia, 1992.

11 DMol^3, www.accelrys.com/cerius2/dmol3.html, 2001.

12 B. Delley, in *Modern density functional theory: a tool for chemistry*, ed. J. M. Seminario and P. Politzer, Elsevier, Amsterdam, 1995, pp. 221–254.

13 B. Delley, *J. Chem. Phys.*, 1990, **92**, 508–517.

14 T. A. Wesolowski, O. Parisel, Y. Ellinger and J. Weber, *J. Phys. Chem.*, 1997, **101**, 7818–7825.

15 I. G. Dance, in preparation for publication.

16 J. P. Perdew and Y. Wang, in *Electronic Structure of Solids 1991*, ed. P. Ziesche and H. Eschrig, Akad. Verlag Berlin, Berlin, 1991, p. 11.

17 J. P. Perdew and Y. Wang, *Phys. Rev. B*, 1992, **45**, 13244–13249.

18 $(Ph_4P)_2[Fe(CN)_5(NO)]$ is isostructural with $(Ph_4As)_2[Fe(CN)_5(NO)]$, reported under reference code PASNTP in the Cambridge Structural Database.

19 G. R. Desiraju and T. Steiner, *The Weak Hydrogen Bond in Structural Chemistry and Biology*, Oxford University Press, Oxford, 1999; T. Steiner, *Angew. Chem., Int. Ed.*, 2002, **41**, 48–76.

20 P. Vitoria, J. I. Beitia, J. M. Gutierrez-Zorrilla, E. R. Saiz, A. Luque, M. Insausti and J. J. Blanco, *Inorg. Chem.*, 2002, **41**, 4396–4404.